Kilometer-range, high resolution depth imaging via 1560 nm wavelength single-photon detection

Article (Published Version)

Kilometer-range, high resolution depth imaging via 1560 nm wavelength single-photon detection

Aongus McCarthy,[1,*] Nils J. Krichel,[1,2] Nathan R. Gemmell,[1] Ximing Ren,[1] Michael G. Tanner,[1,3] Sander N. Dorenbos,[4] Val Zwiller,[4] Robert H. Hadfield,[1,3] and Gerald S. Buller[1]

[1]*Institute of Photonics and Quantum Sciences, and Scottish Universities Physics Alliance (SUPA), School of Engineering and Physical Sciences, Heriot-Watt University, Edinburgh, EH14 4AS, UK*
[2]*Current address: Helia Photonics Ltd, Rosebank Park, Livingston EH54 7EJ, UK*
[3]*Current address: School of Engineering, University of Glasgow, Glasgow, G12 8QQ, UK*
[4]*Kalvi Institute of Nanoscience, Delft University of Technology, 2628 CJ Delft, The Netherlands*
[*]*A.McCarthy@hw.ac.uk*

Abstract: This paper highlights a significant advance in time-of-flight depth imaging: by using a scanning transceiver which incorporated a free-running, low noise superconducting nanowire single-photon detector, we were able to obtain centimeter resolution depth images of low-signature objects in daylight at stand-off distances of the order of one kilometer at the relatively eye-safe wavelength of 1560 nm. The detector used had an efficiency of 18% at 1 kHz dark count rate, and the overall system jitter was ~100 ps. The depth images were acquired by illuminating the scene with an optical output power level of less than 250 μW average, and using per-pixel dwell times in the millisecond regime.

OCIS codes: (110.6880) Three-dimensional image acquisition; (280.3400) Laser range finder; (030.5260) Photon counting; (030.5290) Photon statistics; (120.3930) Metrological instrumentation; (040.3780) Low light level.

References and links

1. M. Amann, T. Bosch, M. Lescure, R. Myllyla, and M. Rioux, "Laser ranging: a critical review of usual techniques for distance measurement," Opt. Eng. **40**(1), 10–19 (2001).
2. C. Mallet and F. Bretar, "Full-waveform topographic lidar: State-of-the-art," ISPRS J. Photogramm. Remote Sens. **64**(1), 1–16 (2009).
3. G. S. Buller and R. J. Collins, "Single-photon generation and detection," Meas. Sci. Technol. **21**(1), 012002 (2010).
4. S. Pellegrini, G. S. Buller, J. M. Smith, A. M. Wallace, and S. Cova, "Laser-based distance measurement using picosecond resolution time-correlated single-photon counting," Meas. Sci. Technol. **11**(6), 712–716 (2000).
5. G. S. Buller and A. M. Wallace, "Ranging and three-dimensional imaging using time-correlated single-photon counting and point-by-point acquisition," IEEE J. Sel. Top. Quantum Electron. **13**(4), 1006–1015 (2007).
6. R. H. Hadfield, "Single-photon detectors for optical quantum information applications," Nat. Photonics **3**(12), 696–705 (2009).
7. W. Becker, *Advanced Time-Correlated Single Photon Counting Techniques* (Springer, 2005).
8. A. McCarthy, R. J. Collins, N. J. Krichel, V. Fernández, A. M. Wallace, and G. S. Buller, "Long-range time-of-flight scanning sensor based on high-speed time-correlated single-photon counting," Appl. Opt. **48**(32), 6241–6251 (2009).
9. C. Ho, K. L. Albright, A. W. Bird, J. Bradley, D. E. Casperson, M. Hindman, W. C. Priedhorsky, W. R. Scarlett, R. C. Smith, J. Theiler, and S. K. Wilson, "Demonstration of literal three-dimensional imaging," Appl. Opt. **38**(9), 1833–1840 (1999).
10. J. J. Degnan, "Photon-counting multikilohertz microlaser altimeters for airborne and spaceborne topographic measurements," J. Geodyn. **34**(3-4), 503–549 (2002).
11. M. A. Albota, B. F. Aull, D. G. Fouche, R. M. Heinrichs, D. G. Kocher, R. M. Marino, J. G. Mooney, N. R. Newbury, M. E. O'Brien, B. E. Player, B. C. Willard, and J. J. Zayhowski, "Three-dimensional imaging laser radars with Geiger-mode avalanche photodiode arrays," Lincoln Lab. J. **13**, 351–370 (2002).
12. B. F. Aull, A. H. Loomis, D. J. Young, R. M. Heinrichs, B. J. Felton, P. J. Daniels, and D. J. Landers, "Geiger mode avalanche photodiodes for three-dimensional imaging," Lincoln Lab. J. **13**, 335–350 (2002).

#183800 - $15.00 USD Received 22 Jan 2013; revised 21 Feb 2013; accepted 21 Feb 2013; published 4 Apr 2013

13. G. S. Buller, R. D. Harkins, A. McCarthy, P. A. Hiskett, G. MacKinnon, G. Smith, R. Sung, A. Wallace, R. Lamb, K. Ridley, and J. Rarity, "Multiple wavelength time-of-flight sensor based on time-correlated single-photon counting," Rev. Sci. Instrum. **76**(8), 083112 (2005).
14. M. G. Tanner, C. M. Natarajan, V. K. Pottapenjara, J. A. O'Connor, R. J. Warburton, R. H. Hadfield, B. Baek, S. Nam, S. N. Dorenbos, E. Urena, T. Zijlstra, T. Klapwijk, and V. Zwiller, "Enhanced telecom wavelength single-photon detection with NbTiN superconducting nanowires on oxidized silicon," Appl. Phys. Lett. **96**(22), 221109 (2010).
15. L. S. Rothman, D. Jacquemart, A. Barbe, D. Chris Benner, M. Birk, L. R. Brown, M. R. Carleer, C. Chackerian, Jr., K. Chance, L. H. Coudert, V. Dana, V. M. Devi, J.-M. Flaud, R. R. Gamache, A. Goldman, J.-M. Hartmann, K. W. Jucks, A. G. Maki, J.-Y. Mandin, S. T. Massie, J. Orphal, A. Perrin, C. P. Rinsland, M. A. H. Smith, J. Tennyson, R. N. Tolchenov, R. A. Toth, J. Vander Auwera, P. Varanasi, and G. Wagner, "The HITRAN 2004 molecular spectroscopic database," J. Quant. Spectrosc. Radiat. Transf. **96**(2), 139–204 (2005).
16. H. Willebrand and B. S. Ghuman, *Free Space Optics: Enabling Optical Connectivity in Today's Networks* (Sams, 2002).
17. S. Pellegrini, R. E. Warburton, L. J. J. Tan, J. S. Ng, A. B. Krysa, K. Groom, J. P. R. David, S. Cova, M. J. Robertson, and G. S. Buller, "Design and performance of an InGaAs-InP single-photon avalanche diode detector," IEEE J. Quantum Electron. **42**(4), 397–403 (2006).
18. N. Namekata, S. Adachi, and S. Inoue, "Ultra-low-noise sinusoidally gated avalanche photodiode for high-speed single-photon detection at telecommunication wavelengths," IEEE Photon. Technol. Lett. **22**(8), 529–531 (2010).
19. M. Ren, X. R. Gu, Y. Liang, W. B. Kong, E. Wu, G. Wu, and H. P. Zeng, "Laser ranging at 1550 nm with 1-GHz sine-wave gated InGaAs/InP APD single-photon detector," Opt. Express **19**(14), 13497–13502 (2011).
20. M. Entwistle, M. A. Itzler, J. Chen, M. Owens, K. Patel, X. D. Jiang, K. Slomkowski, S. Rangwala, and J. C. Campbell, "Geiger-mode APD camera system for single photon 3-D LADAR imaging," Advanced Photon Counting Techniques **VI**, 8375 (2012).
21. M. A. Diagne, M. Greszik, E. K. Duerr, J. J. Zayhowski, M. J. Manfra, R. J. Bailey, J. P. Donnelly, and G. W. Turner, "Integrated array of 2-μm antimonide-based single-photon counting devices," Opt. Express **19**(5), 4210–4216 (2011).
22. P. A. Hiskett, C. S. Parry, A. McCarthy, and G. S. Buller, "A photon-counting time-of-flight ranging technique developed for the avoidance of range ambiguity at gigahertz clock rates," Opt. Express **16**(18), 13685–13698 (2008).
23. C. M. Natarajan, M. G. Tanner, and R. H. Hadfield, "Superconducting nanowire single-photon detectors: physics and applications," Supercond. Sci. Technol. **25**(6), 063001 (2012).
24. R. E. Warburton, A. McCarthy, A. M. Wallace, S. Hernandez-Marin, R. H. Hadfield, S. W. Nam, and G. S. Buller, "Subcentimeter depth resolution using a single-photon counting time-of-flight laser ranging system at 1550 nm wavelength," Opt. Lett. **32**(15), 2266–2268 (2007).
25. N. J. Krichel, A. McCarthy, I. Rech, M. Ghioni, A. Gulinatti, and G. S. Buller, "Cumulative data acquisition in comparative photon-counting three-dimensional imaging," J. Mod. Opt. **58**(3-4), 244–256 (2011).
26. A. N. Bashkatov, E. A. Genina, V. I. Kochubey, and V. V. Tuchin, "Optical properties of human skin, subcutaneous and mucous tissues in the wavelength range from 400 to 2000 nm," J. Phys. D Appl. Phys. **38**(15), 2543–2555 (2005).

1. Introduction

Time-of-Flight (ToF) techniques have played an important role in high-resolution measurement of remote distances. Laser-based ToF approaches have a wide number of end applications, spanning machine vision, navigation for autonomous vehicles and spacecraft, and atmospheric remote sensing [1, 2]. ToF ranging and imaging can be extended to the shot noise limit using detectors with single-photon sensitivity [3] which offers excellent surface-to-surface resolution and an inherent flexibility in the trade-off between acquisition time and depth precision [4, 5]. Innovations in both single-photon detectors [3, 6] and data acquisition technology [7] in recent years have transformed time-correlated single-photon counting (TCSPC) into an advantageous and practical approach to next generation ToF range-finding and depth imaging systems. Recent laboratory and field trial demonstrations have illustrated the benefits of shot-noise limited detection and a picosecond system response in terms of low light sensitivity limits and excellent surface-to-surface resolution [5, 8]. A number of important emerging application areas may benefit from the use of single-photon ToF, especially where remote sensing is a necessary requirement.

Previously, long-range single-photon depth imaging systems have employed micro-channel plate (MCP) detectors [9], photomultipliers (PMTs) [10] or Si-based single-photon avalanche diode (SPAD) detectors [8, 11–13], and as a result all approaches were generally

#183800 - $15.00 USD Received 22 Jan 2013; revised 21 Feb 2013; accepted 21 Feb 2013; published 4 Apr 2013

limited to wavelengths below 1000 nm. We present a new ToF single-photon depth imager, operating at 1560 nm wavelength, which incorporates a free-running, low noise superconducting nanowire single-photon detector (SNSPD) [6] enhanced for detection at wavelengths between 1300 nm and 1560 nm [14]. Using this scanning depth imager, we were able to acquire centimeter resolution depth images of non-cooperative objects (i.e. an object or scene that does not lend itself to reflecting the transmitted laser pulses back towards the source) in daylight at stand-off distances of up to a kilometer using per-pixel dwell times in the millisecond regime. Compared to operation at wavelengths below 1 μm, the 1550 nm region of the spectrum offers lower atmospheric attenuation of the signal [15] and a greatly reduced solar background level [16]. The solar background is typically the dominant source of noise in photon-counting depth imaging systems and the switch in operational wavelength can make long distance, i.e. kilometer range, daylight operation more realizable. In addition, higher laser output power levels can be used at this wavelength while still being eye-safe, and there is less likelihood of detection by electronic counter-measure systems. The measurements reported here were performed using sub-milliwatt average power laser illumination under bright daylight conditions.

Previous research on single-photon ranging and depth imaging systems at similar wavelengths has relied on semiconductor based detectors, mainly electrically-gated InGaAs/InP SPADs [17, 18]. Ren et al [19] used a relatively noisy InGaAs-based SPAD in their 1550 nm wavelength laser ranging system which limited the range measurement to 10's of meters despite milliwatt average laser powers. In contrast to using an individual, high-performance, single-photon counting detector as presented here, other work on single-photon depth imaging has used photon-counting arrays. However, these detector arrays suffered from high dark count rates and relatively poor timing resolution, and resulted in shorter range and lower depth resolution than we report here. For example, 32 × 32 arrays of InGaAsP and InGaAs-based Geiger-mode (GM) avalanche photodiode (APD) arrays were designed for single-photon laser depth imaging at a wavelength of either 1.06 μm or 1.55 μm [20]. MIT Lincoln Laboratory used a GaSb-based material system 32 × 32 GM APD array to extend to 2 μm wavelength operation, achieving 30 cm depth resolution at a distance of 20 meters [21].

2. System description

A schematic of our depth imaging system is shown in Fig. 1, and the main system details are summarized in Table 1. The scanning transceiver was adapted from previous work at 842 nm wavelength [8], and reconfigured for use at 1560 nm.

A mode-locked fiber laser with a central wavelength of 1560 nm, a pulse repetition rate of 50 MHz, a pulse width of <1 ps, and a typical maximum average output power of 2 mW was employed as the illumination source. Due to the range ambiguity effects of high frequency periodic illumination caused by multiple indistinguishable illumination pulses in transit at any given point, the 50 MHz periodic repetition rate of the laser meant that we were limited to making depth profiling measurements rather than absolute depth measurements. Future work will implement the use of pseudorandom pulse trains in order to overcome this range ambiguity issue found at high laser repetition rates [22]. The output light from the 90% channel of a fiber splitter was coupled into the transmit channel of the scanning transceiver. The 10% output channel from the fiber splitter was directed to a trigger detector (i.e. a commercial InGaAs APD), whose output was used as the start signal for the TCSPC [7] hardware module. This start trigger signal, with a frequency of 50 MHz, was electrically down-divided to a frequency of 1.57 MHz in order to match the working range of the TCSPC module. This module had 20 ps Full Width at Half Maximum (FWHM) jitter and was configured with a 16 ps time bin width.

#183800 - $15.00 USD Received 22 Jan 2013; revised 21 Feb 2013; accepted 21 Feb 2013; published 4 Apr 2013

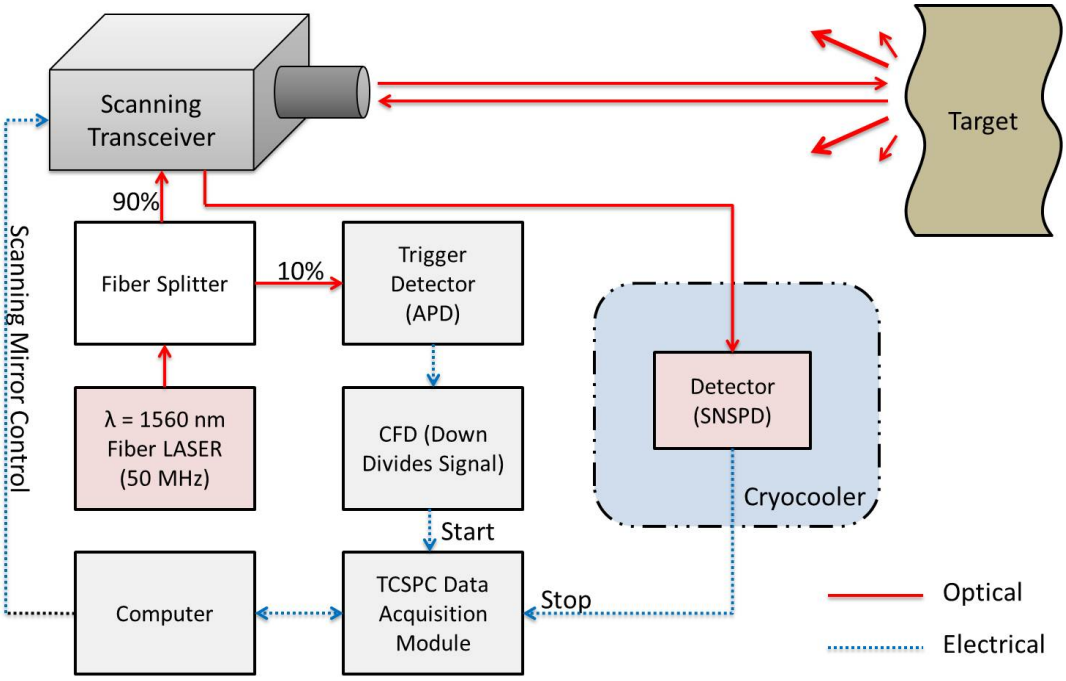

Fig. 1. Schematic of the photon-counting depth imaging system based on sub-picosecond 1560 nm wavelength illumination and a superconducting nanowire single-photon detector (SNSPD). CFD, constant fraction discriminator; APD, avalanche photodiode; TCSPC module, time correlated single-photon module.

Table 1. Summary of the Main System Parameters

System Parameter	Comment
Transmit/Receive Alignment	Monostatic: Coaxial transmit and receive channels.
Laser	Mode-locked fiber laser based on a CNT-1560 laser engine by Kphotonics
Laser Repetition Rate	50 MHz
Illumination Wavelength	1560 nm
Laser Pulse Width	<1 ps
Objective Lens	500 mm focal length cemented achromatic doublet, 80 mm diameter aperture, no anti-reflection coating.
Average Output Power	< 250 μW exiting the system
Range	Scans performed at 325 meters, 910 meters, and 4.4 km
Beam Scanning Mechanism	Galvanometer controlled mirrors (x & y) common to transmit and receive channels
Spectral Filters	Longpass: 1500 nm cut-on Bandpass: 12 nm Full Width at Half Maximum (FWHM), 1560 nm center wavelength
Collection Fiber	9 μm diameter core (SMF28), 2 meters long, armored
Detector	NbTiN SNSPD in resonant cavity geometry, ~18% quantum efficiency at λ = 1560 nm with 1 kHz dark count rate. Operated at a temperature of ~3K
System Temporal Response (jitter)	~98 ps FWHM
System Spatial Resolution (x-y)	~50 μrad
Data Acquisition Hardware	PicoQuant PicoHarp 300

#183800 - $15.00 USD Received 22 Jan 2013; revised 21 Feb 2013; accepted 21 Feb 2013; published 4 Apr 2013

A pair of galvanometer mirrors in the transceiver enabled the laser beam to be raster scanned across the target scene under computer control. The transmit and receive channels of the custom scanning transceiver were coaxial and the two galvanometer mirrors were common to both channels. These channels were separated via a polarizing beamsplitter only after the return signal had reflected from both galvanometer mirrors. The objective lens was a cemented achromatic doublet with a focal length of 500 mm and an 80 mm diameter aperture. The scattered target return collected by the transceiver was spectrally filtered as detailed in Table 1. The collected photon flux from the receiver channel of the scanning transceiver was delivered to a superconducting nanowire single-photon detector (SNSPD) system [23] via a 2 meter long armored single mode optical fiber. This generated a stop trigger pulse for the TCSPC module. In all the measurements reported here the average emitted optical power was less than 250 μW.

We employed a niobium titanium nitride (NbTiN) SNSPD on an oxidized silicon substrate, forming a resonant optical cavity to achieve improved detection efficiency at telecom wavelengths [14]. The SNSPD was coupled using single-mode telecommunications optical fiber (9 μm diameter core) and mounted inside a closed-cycle refrigerator system [23] eliminating the need for liquid cryogens and making this advanced detector technology viable for these field trials. The detector was maintained at an operating temperature of ~3 K and when biased at a level consistent with a 1 kHz dark count rate, the SNSPD had a practical efficiency of 18% at 1560 nm wavelength. Output voltage pulses from the SNSPD were amplified (580 MHz 3dB roll off) outside the cryostat at room temperature and routed to the TCSPC module.

Spatial and spectral filtering of the return signal within the transceiver unit ensured that even under bright daylight conditions, the solar background level was limited to a maximum of approximately 8 kHz. The overall system instrumental timing response of the system was <100 ps FWHM (see the inset in Fig. 2) which was, owing to the increased complexity of this transceiver setup, marginally longer than the timing resolution achieved in our first 1550 nm wavelength single photon depth ranging tests with SNSPDs [24].

The detected photon events were time-tagged by the TCSPC module and continuously streamed to the control computer. Software reconciled this photon return timing with field position in order to calculate depths at individual target positions, producing a depth image of the scanned optical field. An instrumental reference response was constructed by taking a histogram from retro-reflective material over a long integration time (using the same 16 ps bin width as in the scan measurements), a peak from which was then isolated and normalized in height, shown in the inset of Fig. 2. A cross-correlation algorithm written in house (based on that presented in [25]) analyses the histogram for each pixel in a scan. It begins by preparing a periodic reference response, R, of equal length to the histogram, H, containing multiple versions of the instrumental reference peak spaced equally at the period of the fiber laser's output. A cross correlation, C can then be calculated via: $C = F^{-1}[F(H) \,.\times F^*(R)]$, where F denotes fast Fourier transform, and $.\times$ denotes element-wise multiplication. An example of C is shown in Fig. 2. The calculation of $F^*(R)$ is performed only once per scan to speed up processing. This cross correlation discriminates against random noise peaks, amplifying the probability of finding a target return signal amongst noise. The algorithm checks for a peak within the cross correlation by looking for the highest signal within the time window which does not contain any back reflections (determined by the user), and outputs the position of its maximum. This position can then be converted from bin number (time) into a distance. A 4500 pixel depth image, such as those in Fig. 3, was processed in under two minutes on a standard desktop computer.

#183800 - $15.00 USD Received 22 Jan 2013; revised 21 Feb 2013; accepted 21 Feb 2013; published 4 Apr 2013

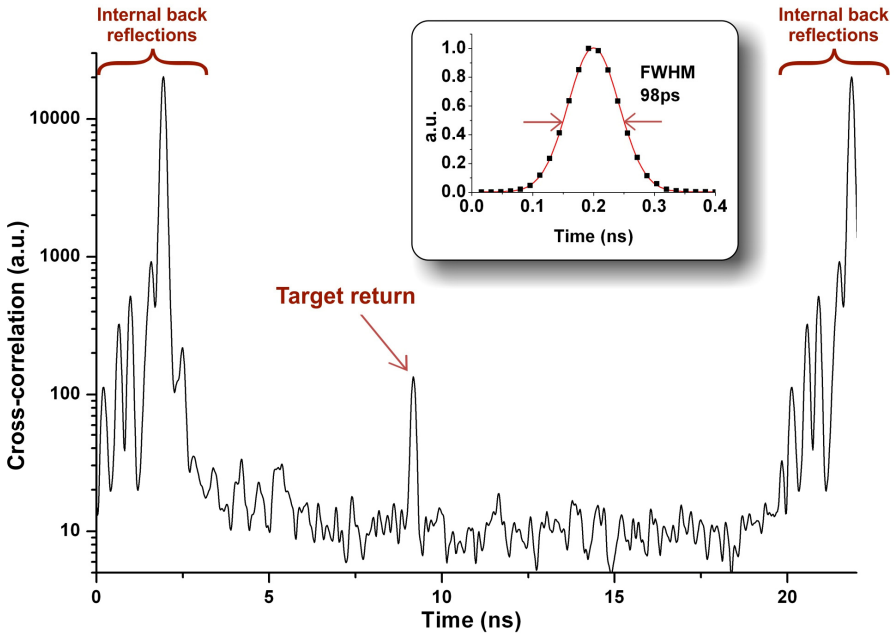

Fig. 2. Processed histogram by cross-correlation method. Example of the cross-correlation function C of a processed pixel showing the return peak (at approximately 9 ns) standing clearly above the background. Also present are the internal back reflections from the scanning system. The inset shows a normalized instrumental response of the system with 98 ps Full Width at Half Maximum (FWHM) timing jitter.

3. Experiments and results

We used a clothed, life-size mannequin as a target object for initial field trials. Figure 3 shows scans of the same scene acquired at a stand-off distance of 325 m in daylight conditions, using different per-pixel dwell times. The depicted surface plots clearly demonstrate reliable target resolution at dwell times as short as 1 ms per pixel; even at the shortest per-pixel dwell time of 0.5 ms, the majority of the depth pixels were resolved correctly. At long dwell times, the uncertainty on the per-pixel target return intensity is low enough to convey another layer of information. The surface plot's color mapping can be set to correspond to the calculated number of detected return photons in the histogram peak for each individual pixel – this is shown in the 10 ms per pixel intensity images in Figs. 4(c) and 4(f). Clear intensity differences are evident, based on the material type and the angle of the surface relative to the incident beam. It is apparent from the depth image shown in Fig. 4(e) that the returns from human skin were very low in comparison to the other materials, resulting in the majority of the facial pixels having insufficient detected return photons to provide depth information for this acquisition duration when illuminated with 1560 nm wavelength. This is consistent with the findings of Bashkatov et al. who report reduced scattering from human skin and subcutaneous tissue at wavelengths in the vicinity of $\lambda = 1550$ nm when compared to $\lambda = 850$ nm [26].

#183800 - $15.00 USD Received 22 Jan 2013; revised 21 Feb 2013; accepted 21 Feb 2013; published 4 Apr 2013

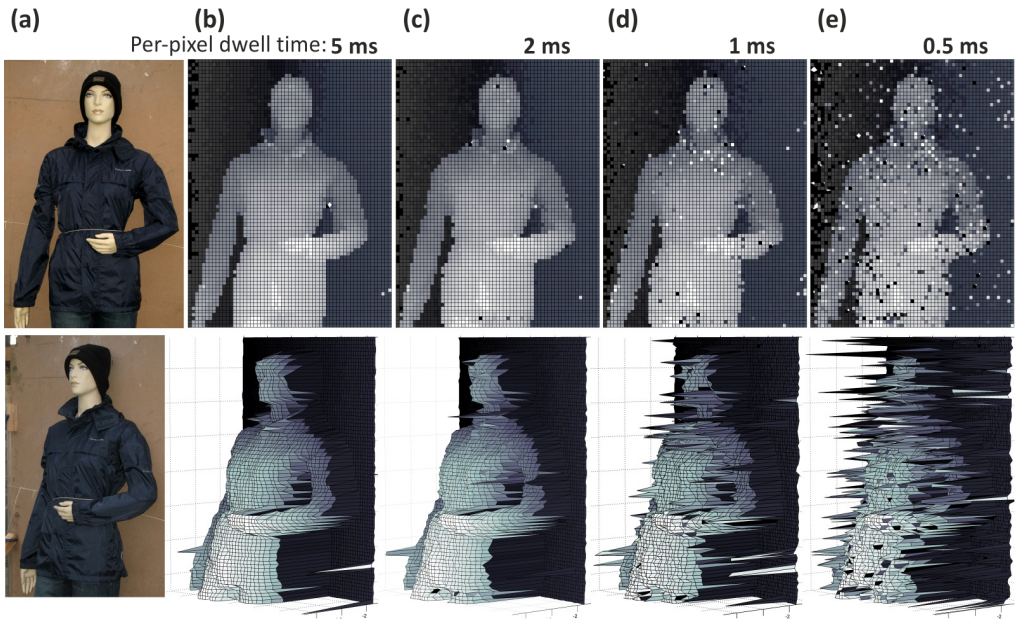

Fig. 3. Depth profile measurements made in daylight on a life-size mannequin from a standoff distance of 325 meters. The images shown in column (a) are close-up photographs showing different viewpoints of the scene which consisted of the mannequin against a hardboard backplane. The depth scans were acquired in daylight and each scan covered an area of approximately 800 × 1000 mm using 60 × 75 pixels, resulting in a pixel-to-pixel spacing of approximately 13 mm in x and y. Plots of the depth data obtained for per-pixel acquisition times of 5, 2, 1, and 0.5 ms are shown in columns (b) through (e) – each of these columns show two different viewpoints of the surface plot constructed from the data obtained using the specified per-pixel dwell time. A per-pixel dwell time of 1 ms equated to a total scan time of 4.5 s for this scene. The face-on view shown in the top row gives an indication of the spatial resolution of the system, and the centimeter-scale depth resolution can be gauged from the oblique view in the bottom row. The color shading in the plots is used to map depth, and the images are surface plots of the raw depth data for all pixels i.e. no curve fitting or extrapolation has been applied to enhance the data returned by the system.

#183800 - $15.00 USD Received 22 Jan 2013; revised 21 Feb 2013; accepted 21 Feb 2013; published 4 Apr 2013

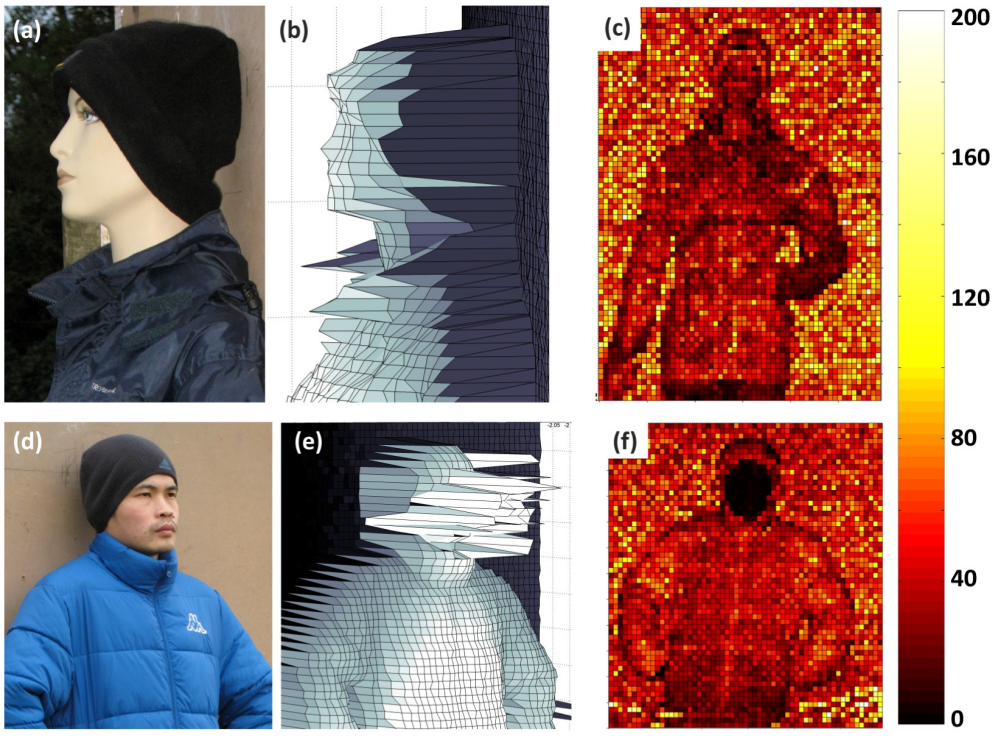

Fig. 4. Comparison between the results obtained from scans, of a mannequin and a human, at a range of 325 meters using a per-pixel dwell time of 10 ms. A close-up photo of the mannequin's head is shown in (a), and the surface plot of depth data acquired at a range of 325 meters with a 10 ms per-pixel dwell time is shown from a similar viewpoint in (b). The plot shown in (c) uses color to map the calculated number of detected return photons in the histogram peak for each individual pixel. At per-pixel dwell times of 10 ms and greater, almost all of the pixels in this scene had sufficient detected photons to provide a true depth reading at this range as is evident from the centimeter-scale features evident in (b). However, the detected photon returns from human skin were significantly lower at this wavelength. The scene shown in (d) of one of the co-authors was scanned with a 10 ms per-pixel dwell time and the surface plot in (e) was obtained – in this case, most of the facial pixels had insufficient detected photons for the determination of a depth. The low number of detected return photons from the facial skin is obvious on the corresponding color map shown in (f). The plots in (c) and (f) also confirm that there are lower returns from the areas of the scene that the illuminating beam strikes at glancing angles e.g. edges.

In order to assess the performance of our system over kilometer-scale distances we carried out measurements using an available 910 meter range, with the mannequin and members of our team again posing as targets. Figure 5 shows three different viewpoints of the depth data obtained of the mannequin at different per-pixel dwell times. The frontal perspective of the depth images, shown in the top row, gives a visual indication of the xy centimeter-scale spatial resolution that was achieved at this range, and illustrate that different shapes and forms can be easily identified even at per-pixel acquisition times as low as 2 ms. Figure 6 shows members of the research group posing for depth profile scans at the standoff distance of 910 meters at per-pixel acquisition times of 50 ms and 10 ms. Depth features on the centimeter scale, such as folds in the clothing, are clearly evident in all of the depth images shown in Fig. 5 and Fig. 6. However, as was mentioned about the results shown in Figs. 4(e) and 4(f), it is evident from the depth images shown in Figs. 6(b) and 6(d) that the returns from human skin were relatively low.

#183800 - $15.00 USD Received 22 Jan 2013; revised 21 Feb 2013; accepted 21 Feb 2013; published 4 Apr 2013

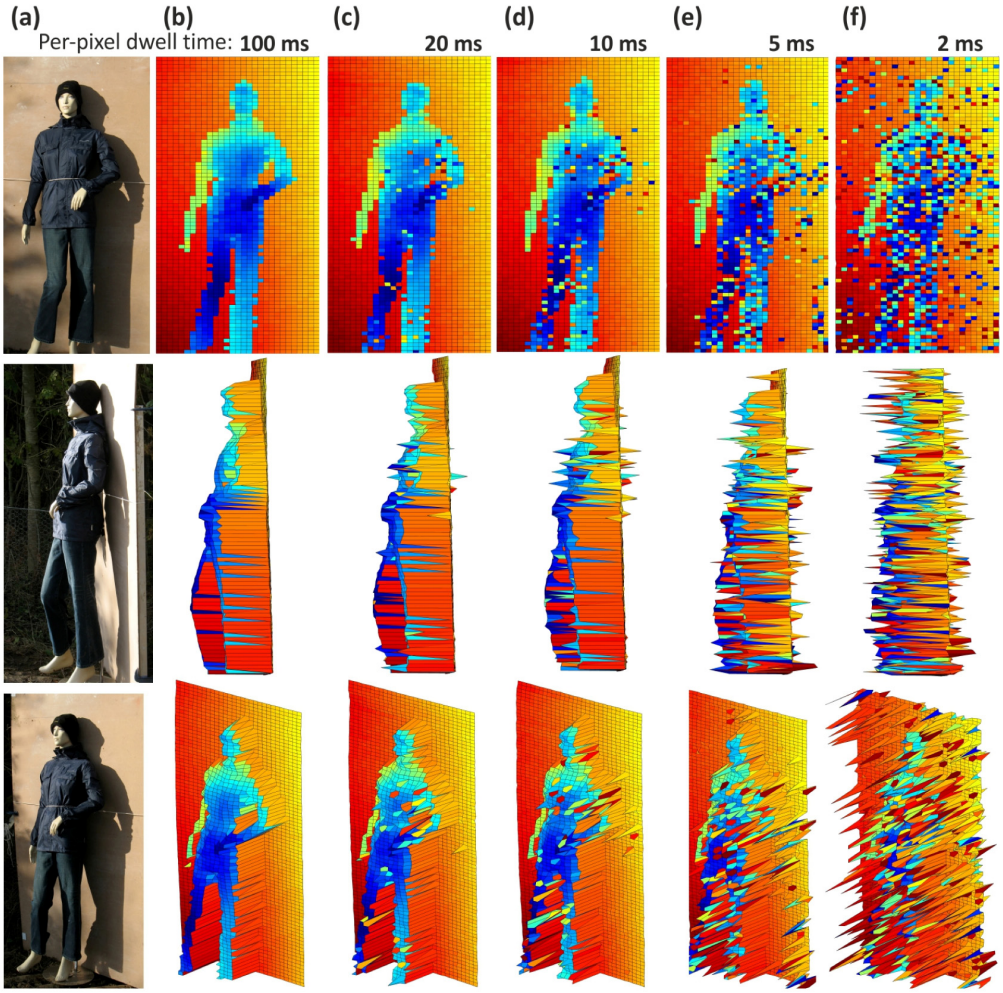

Fig. 5. Depth profile measurements made in daylight of a life-size mannequin from a standoff distance of 910 meters. The close-up photographs in column (a) are different viewpoints of the scene that was scanned which consisted of the mannequin against a hardboard backplane. The depth scans were acquired in daylight and each scan covered an area of approximately 800 × 2000 mm using 30 × 80 pixels, resulting in a pixel-to-pixel spacing of approximately 25 mm in x and y. Surface plots of the raw depth data obtained for per-pixel acquisition times of 100, 20, 10, 5, and 2 ms are shown in columns (b) to (f) - each of these columns show three different views of the data obtained with the specified per-pixel dwell time. A per-pixel dwell time of 10 ms equated to a total scan time 24 s for this scene. The color is used to map depth. The face-on view shown in the top row gives an indication of the spatial resolution of the system at a kilometer, and the centimeter scale depth resolution can be gauged from the oblique and side-on views in the bottom two rows.

#183800 - $15.00 USD Received 22 Jan 2013; revised 21 Feb 2013; accepted 21 Feb 2013; published 4 Apr 2013

Fig. 6. Depth profile measurements of humans, acquired in daylight at a standoff distance of 910 meters. The close-up photographs in columns (a) and (c) are different viewpoints of the scenes which were scanned – two of the authors posed in front of a sheet of hardboard. The depth scans were acquired in bright daylight and each scan covered an area of approximately 800 × 2000 mm using 40 × 80 pixels, corresponding to a maximum field of view of 2 mrad. Surface plots of the raw depth data obtained are shown in columns (b) and (d) - these columns show two different views of the data obtained with the specified per-pixel dwell time. It took 32 seconds to acquire the data shown in (d). The color shading in the surface plots is used to map depth.

We also performed daylight measurement on a scene at a standoff distance of 4400 meters. A 20 × 12 pixel scan was carried out on an area measuring approximately 2000 × 1200 mm, as shown from different viewpoints in Fig. 7. Sub-centimeter depth resolution was achieved, using a per-pixel dwell time of 2 seconds, for the parts of the scene containing co-operative targets e.g. retro-reflective material similar to that used for car license plates. At this range, the spatial resolution was judged to be approximately 250 mm. Of course, these relatively long acquisition times would be reduced with higher laser power which was not available in these initial trials.

#183800 - $15.00 USD Received 22 Jan 2013; revised 21 Feb 2013; accepted 21 Feb 2013; published 4 Apr 2013

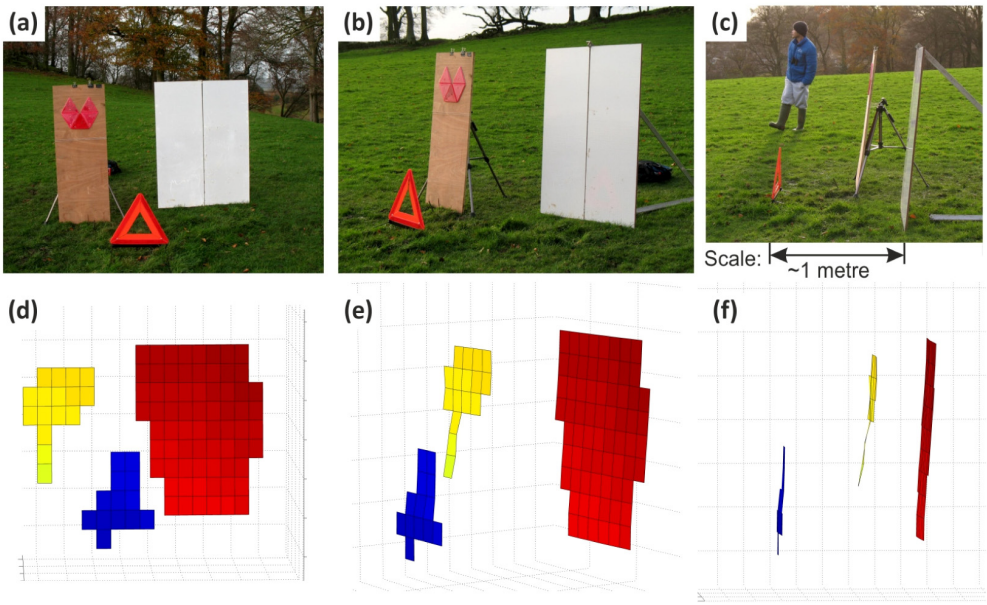

Fig. 7. Depth profile measurement made on a scene from a standoff distance of 4400 meters in broad daylight. The photographs (a), (b) and (c) are different viewpoints of the scene that was scanned with (a) being the view as seen from the approximate direction of the transceiver. The scene consisted of 1.2 meter tall boards with retro-reflective material (one plywood panel with a set of five red retro-reflecting triangles, and two adjoining panels covered in white retro-reflecting material), and a 400 mm tall red retro-reflective roadside warning triangle. The distance between the base of the white panels and the base of the red retro-reflective warning triangle was approximately 1 meter, as indicated in (c). The per-pixel acquisition time was 2 seconds. The surface plot of the 20 × 12 pixel depth data is shown from three different viewpoints in (d), (e) and (f), nominally corresponding to the viewpoints of the photographs.

The achievable pixel-to-pixel depth uncertainty at the stand-off distances of 325, 910, and 4400 m was investigated by scanning a planar target surface covered in retro-reflective material. Mathematical planes were fitted to the surface pixels of the acquired data, and the standard deviation of the pixel residuals served as an indicator of the system depth resolution. A per-pixel dwell time of 1 ms resulted in a pixel-to-pixel depth uncertainty of 0.8 mm for the 325 m range. Using a per-pixel dwell time of 10 ms for the 910 meter range, and 2 seconds for the 4400 meter range, yielded depth residuals of 1.1 mm and 1.5 mm respectively.

These rapid acquisition times enabled us to record a 1 mrad field-of-view depth profile movie of a moving object at a standoff distance of 325 m using a pixel dwell time of 1 ms. This four-second movie, Fig. 8 (Media 1), has centimeter resolution in xyz and was captured in daylight at 10 frames per second, each frame having 10 × 10 pixels.

4. Conclusions

We have presented a ToF scanning depth imaging system operating at an illumination wavelength of 1560 nm and using a superconducting nanowire single photon detector. The high infra-red efficiency of the SNSPD allows the system to incorporate existing optical telecommunications component technology, while also operating in a spectral band with reduced atmospheric attenuation and lower solar background. Low-signature, non-cooperative targets were raster scanned under bright daylight conditions at standoff distances up to 910 m using eye safe low average power illumination. This approach has facilitated the acquisition of depth profile images with millimeter-scale depth resolution – far beyond the capabilities of other current single-photon approaches at such ranges. These results demonstrate the flexibility of the TCSPC technique in negotiating the trade-offs between depth resolution,

#183800 - $15.00 USD Received 22 Jan 2013; revised 21 Feb 2013; accepted 21 Feb 2013; published 4 Apr 2013

data acquisition times and optical power. Using an average laser power of less than 1 mW excellent frame rates have been achieved; higher power sources can be utilized in future for higher frame rates or improved depth resolution whilst still maintaining entirely eye-safe operating conditions.

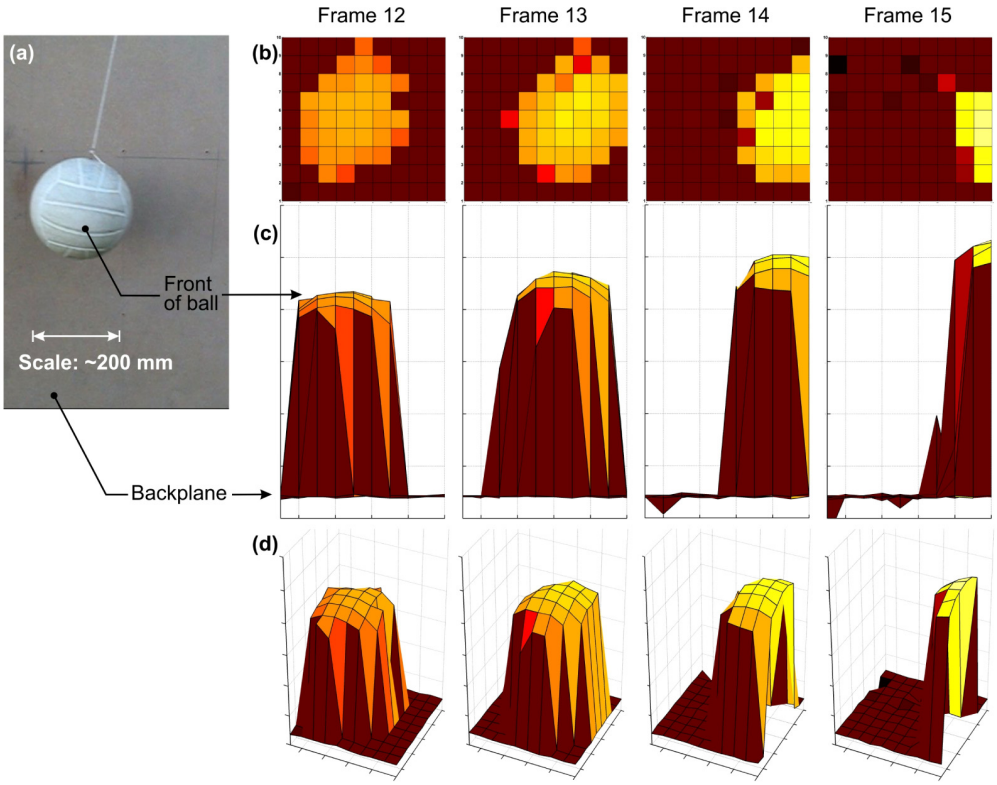

Fig. 8. Time-of-flight depth profile movie, recorded in daylight, of a scene from a standoff distance of 325 meters (Media 1). The image shown in (a) is a close-up photograph of the scene which consisted of a ~200 mm diameter soccer ball suspended in front of a hardboard backplane. The "ball pendulum" was set in motion with the plane of the oscillation at an angle to the backplane. A four-second movie was recorded in daylight at 10 frames per second - each frame had 10 × 10 pixels, and consequently a per-pixel dwell time of 1 ms. The data acquired for four consecutive frames (numbers 12 to 15) is shown. The columns labeled *Frame 12* to *Frame 15* show three different views of the plotted raw depth data for each frame - row (b) is a front view, row (c) is a top-down view, and row (d) is an oblique view. Color is used to map depth and is consistent across all of the plots. The curvature of the front surface of the ball is clearly evident in the depth profile views shown in rows (c) and (d), as is the increasing separation between the ball and the backplane when moving from frame 12 to frame 15.

Acknowledgments

GSB and RHH thank the UK Engineering and Physical Sciences Research Council for support (Platform Grant Award: EP/F048041/1). RHH acknowledges a Royal Society of London University Research Fellowship. The team from Heriot-Watt University is affiliated to the Scottish Universities Physics Alliance (SUPA) and thanks Peter Heron for technical support with the mechanics of the system. VZ and SD acknowledge funding support from the Netherlands Organization for Scientific Research (NWO) and the Netherlands Foundation for Fundamental Research on Matter (FOM).